
Measurement of Temperature and Velocity Fields of Freezing Water using Liquid Crystal Tracers

Tomasz A. Kowalewski

Polish Academy of Sciences, IPPT PAN,
Center of Mechanics and Information Technology,
Swietokrzyska 21, PL 00-049 Warszawa, Poland

Abstract. A new experimental technique based on a computational analysis of the colour and displacement of thermochromic liquid crystal tracers was applied to determine both the temperature and velocity fields of freezing water. The technique combines Digital Particle Image Thermometry and Digital Particle Image Velocimetry. Full 2-D temperature and velocity fields are determined from a pair or a longer sequence, of colour images taken for the selected cross-section of the flow.

1 Introduction

Application of numerical methods for freezing problems necessitate the solution of non-linear partial differential equations of fluid variable properties coupled with moving solid/liquid interfaces. Due to the complexity of the problem, it is not a trivial task to determine precisely an error in the numerical results. The limited accuracy of different numerical methodologies and inevitable simplifications introduced in the models are usually difficult to predict a priori [1]. Hence, the experimental verification of numerical models has special importance for phase change problems. For the same reason, full field measurements of velocity and temperature become crucial for flow problems accompanied by phase changes. With this objective in view, a new experimental technique based on a computational analysis of the colour and displacement of thermochromic liquid crystal tracers (TLCs) was applied to determine both the temperature and velocity fields of the flow. The method combines Digital Particle Image Thermometry and Digital Particle Image Velocimetry. Full 2-D temperature and velocity fields are determined from a pair or a longer sequence of colour images taken for the selected cross-section of the flow.

2 Particle Image Thermometry and Velocimetry

Liquid crystals are highly anisotropic fluids that exist between the boundaries of the solid phase and the conventional isotropic liquid phase. Thermochromic Liquid crystals are temperature indicators that modify incident white light.

The displayed colour is proportional to temperature: red at the low temperature margin of the colour-play interval and blue at the high end. The colour change is reversible and is the basis of numerous applications of TLCs in heat transfer studies. Several types of TLC foils or paints are available for the measurement of the surface temperature. The application of TLCs as tracers opens a new possibility of instantaneous full field measurements of temperature and velocity in thermally driven flow. Liquid crystals dispersed into the liquid become small thermometers monitoring the local fluid temperature [2].

For flow visualization the classical “light sheet” technique is used. The collimated source of white light illuminates the selected cross-section of the flow and colour images are acquired in the perpendicular direction. Illuminated TLC-tracers appear on images as clouds of coloured spots conveyed by the fluid. Digital acquisition of the images allows quantitative measurement of both the temperature and displacement of the tracers. The temperature measurements are based on a digital colour analysis of RGB^1 images. The RGB representation of the colour can be transformed to other *trichromic decomposition*. The choice of the colour space is not unique, several standards have been developed, especially for the colour television or printing applications. For evaluating the temperature so called HSI^2 representation of the RGB colour space is the most favourable. The hue (chromaticity) represents the dominant wavelength of the colour and its value which depends directly on the TLCs temperature. The light intensity (or brightness) is defined simply as a sum of its three primary components: $I = \sqrt{(R^2 + G^2 + B^2)}/3$. For the 8-bit representation the maximum intensity is equal 255. Saturation represents colour purity. It can be easily found as a remainder after subtraction of white background from the light intensity: $S = 255 \cdot (1 - \min(R, G, B)/I)$. Pure colours have saturation equal 255. The hue value is calculated as a normalized value of the dominating colour. To make use of the 8-bit signal dynamics and limiting ourselves to the spectral colours, the following formula is used to calculate the hue value:

$$H = \begin{cases} 63 + ((G' - R') \cdot 63)/(G' + R') & \text{for } B' = 0 \\ 189 + ((B' - G') \cdot 63)/(B' + G') & \text{for } R' = 0 \end{cases} \quad (1)$$

where, $R' = R - \min(R, G, B)$, similar for G' and B' .

The incoming RGB signals from the video camera are transformed pixel by pixel into hue, saturation and intensity. The red, green and blue colours correspond to the hue values of 0, 126 and 252, respectively. The temperature is determined by relating the hue to a temperature calibration function. Our 8-bit representation of the hue value ensures resolution better than 1%. However, the colour-temperature relationship is strongly non-linear (Fig. 1). Hence, the accuracy of the measured temperature depends on the colour

¹ Red, Green and Blue intensities produces by a video camera

² Hue, Saturation and Intensity

(hue) value. The relative error, based on the temperature range defined by the TLCs colour-play limits, varies from 3% to 10%. For the TLCs used (TM from Merck) there results an absolute accuracy of 0.15°C for lower temperatures (red-green colour range) and 0.5°C for higher temperatures (blue colour range). The most sensitive region is the colour transition from red to green which takes place over a temperature variation of less than one degree Celsius. To improve the accuracy of temperature measurements, some experiments were repeated using four different types of TLCs, so that their combined colour-play range covered temperatures from -5°C to 14°C .

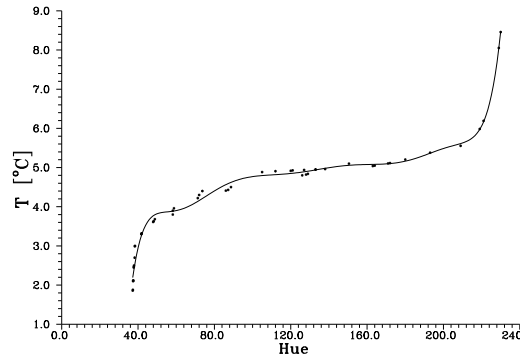


Fig. 1. Temperature vs. Hue for TLCs used. Calibration curve is obtained by 8th order polynomial fitted to the experimental points

The 2-D velocity vector field was measured by Digital Particle Image Velocimetry (DPIV). By this method, the motion of the TLC tracers observed in the plane of the illuminating light sheet, is analysed. To improve contrast and amplify intensity of the particle images a special filtering technique is applied. It is based on a local analysis of the average intensity within small (3x3 pixel) windows. Pixels with intensity well above the average are treated as particles and their intensity is amplified. In such a way bright images of the tracers with preserved intensity variation, well suited for DPIV, are obtained. In the classical DPIV analysis the magnitude and direction of the velocity vectors are determined by using an FFT-based cross-correlation between small sections (interrogation windows) of one pair of images taken at the given time interval. The spatial resolution of the method is limited by the minimum number of tracers present in the interrogation window. Further improvement in the evaluation accuracy allows the recently developed ODP-PIV³ method of image analysis [3]. Due to an iterative search algorithm used, a dense velocity field is obtained, with displacement value calculated at each image pixel. The accuracy of the FFT-based DPIV and that of the ODP-

³ Orthogonal Dynamic Programming - Particle Image Velocimetry

PIV method is 0.6 pixels and 0.15 pixels, respectively. This means that for a typical displacement vector of 10 pixels the relative accuracy of the velocity measurement (for a single point) is better than 6%.

3 Problem Formulation and Experimental Procedure

We consider convective flow of freezing water in a simple geometry, a cube shaped cavity of 38mm internal size. One of its walls is held at a temperature of -10°C . As it is below the freezing temperature of the water, hence ice forms there. Two configurations are investigated. In the first, flow develops in the cavity with a horizontal temperature gradient between two opposite isothermal walls (Fig. 2a). One of the isothermal walls has a temperature of 10°C , the other one -10°C . The cavity is surrounded by air at room temperature (25°C). The remaining four walls, made of 6mm thick Plexiglas, are nominally insulators. The thermal conductivity of Plexiglas is three times smaller than that of water. However, it appears that even that small thermal conductivity of the side walls has an apparent effect on the development of fine flow structures and must be considered in numerical simulations.

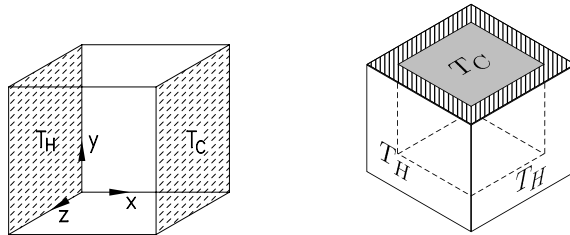


Fig. 2. Differentially heated Plexiglas cavity with the two metal walls kept at temperatures T_h and T_c (*left*). Lid cooled cavity with the metal lid kept at temperature T_c , and five Plexiglas walls surrounded by external fluid at temperature T_h (*right*)

In the second configuration (Fig. 2b), the top wall of the cavity is isothermal and kept at the low temperature $T_c = -10^{\circ}\text{C}$. The other five walls are non-adiabatic, made of 8mm thick Plexiglas. The cavity is immersed in an external water bath kept at temperature $T_h = 20^{\circ}\text{C}$. Due to forced convection in the bath it can be assumed that the temperature at the external surfaces of the box is close to the bath temperature. Because of the final conductivity of Plexiglas the temperature field at the inner surfaces of the walls adjusts itself, depending on both the flow inside the box and the heat flux through and along the walls.

The experimental apparatus used consists of a convection box, a halogen tube lamp, a 3-chip colour CCD camera (Sony XC003) and a 32-bit PCI-bus frame grabber (AM-STD ITI). The flow field is illuminated with a 2mm

thick sheet of white light from a specially constructed halogen lamp, and observed in the perpendicular direction. The temperature of the isothermal walls and that of the water in the bath (eventually surrounding the cavity) are controlled by thermostats. The computer controlled system of three stepping motors allows the acquisition of images of several cross-sections, both for horizontal and vertical planes, fully automatically within several seconds. This allows a three-dimensional analysis of the whole flow domain. The computer also controls switching of the halogen lamp and records readings from four control thermocouples and the thermostats. A fine dispersion of raw liquid crystal material was used as tracers. Their mean diameter is about $50\mu\text{m}$. To get a general view of the flow pattern, several images recorded periodically within a given time have been added in the computer memory.

4 Selected Results

4.1 Differentially heated cavity

The two opposite metal walls of the cube are assumed to be isothermal. Due to temperature gradients existing between the walls the recirculating flow is generated in the cavity. This flow configuration resembles a popular “bench mark” case, natural convection in a cubical cavity with differentially heated end walls. However, the behaviour of natural convection of water in the vicinity of the freezing point creates interesting and also difficult features for numerical modelling of flow structures. It is mainly due to the strongly non-linear temperature dependence of the density function with the extremum at 4°C . The competing effects of positive and negative buoyancy force result in a flow with two distinct circulations (Figs. 3,4). There is “normal” clockwise circulation, where the water density decreases with temperature (upper-left cavity region) and “abnormal” convection with the opposite density variation and counter-clockwise rotation (lower-right region). At the upper part of the cold wall the two circulations collide with each other, intensifying the heat transfer and effectively decreasing the interface growth. Below, the convective heat transfer from the hot wall is limited by the abnormal circulation, separating it from the freezing front. Hence, the phase front is only initially flat. As time passes it deforms strongly, getting a characteristic “belly” at its lower part. This type of flow structure appeared to be very sensitive to thermal boundary conditions at the side walls. Despite improvements in the numerical model we used, the computational results differ in detail from their experimental counterparts [4]. An eventual source of observed discrepancies could be the supercooling of water, which delays creation of the first ice layer and deforms the flow pattern at the top of the cavity (comp. Fig. 3a). It is well known that pure water may supercool as far as -40°C , before freezing occurs. Seeding of the flow with thermochromic liquid crystals allowed us to visualize that in fact initial water temperature reaches about -7°C before freezing starts.

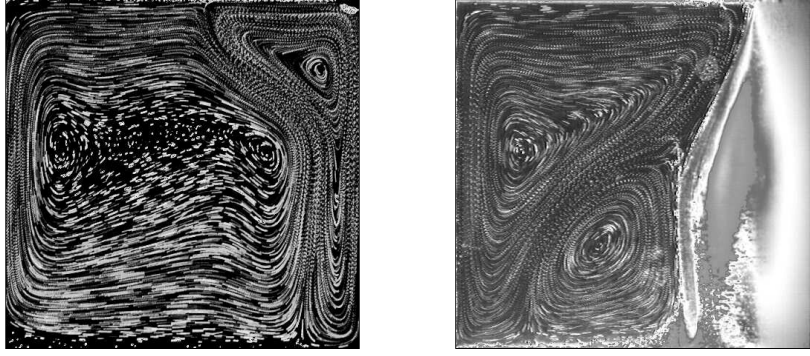


Fig. 3. Flow structure observed for the centre plane ($z=0.5$) in the differentially heated cavity at 60s (*left*) and 2600s (*right*) after cooling started

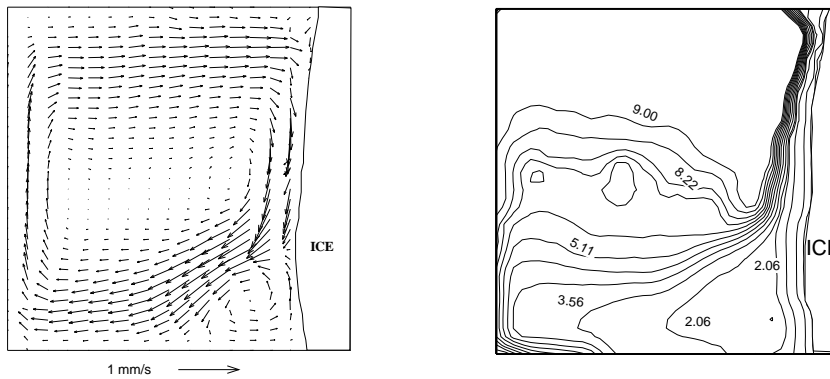


Fig. 4. Velocity (*left*) and temperature isotherms (*right*) field evaluated for water freezing in the differentially heated cube at 500s, $T_h=10^\circ\text{C}$, $T_c=-10^\circ\text{C}$

4.2 Lid cooled cavity

The problem of melt-flow in a lid-cooled cavity has a practical application in a number of manufacturing processes and physical situations. A large scale example is the freezing of water reservoirs, where at night, cooling from above initiates freezing and generates convective flow beneath the ice. On a smaller scale, it has been recognized in crystal growth problems that the flow pattern beneath the solidifying surface is of critical importance to crystal quality. The occurrence of convective flow in the presence of vertical temperature gradients is known to be stable only within a relatively narrow range of Rayleigh number. In our experiments on a lid-cooled cavity there was heat flux into the liquid through the sides and bottom walls. It has been found that these boundary conditions have a stabilising effect on the overall flow, and sta-

ble flow structures are possible at $Ra > 10^6$, well above the second critical number for the Rayleigh-Bénard instability. However, various modes of instabilities are observed during the onset of convection. Before a stable final flow structure is achieved, several oscillatory changes in its pattern are observed [5]. The initial flow instabilities, clearly visible in the TLCs visualized temperature field, are also reproduced in the numerical simulations [6]. When a phase change takes place, in our case freezing on a lid surface, strongly non-linear coupling of the flow and interface is responsible for the interface geometry. Despite the fact that freezing starts at a planar surface, the ice surface does not remain planar. Its distortion in turn affects the convection in the whole cavity. A complex interaction between the flow, the moving boundary and the latent heat removed at the solid/liquid interface determines the flow pattern which is established. Fig. 5 shows the temperature and velocity field evaluated for the quasi-steady state, i.e. 5 hours after the experiment was started. The flow visualisation performed in the lid cooled cavity shows

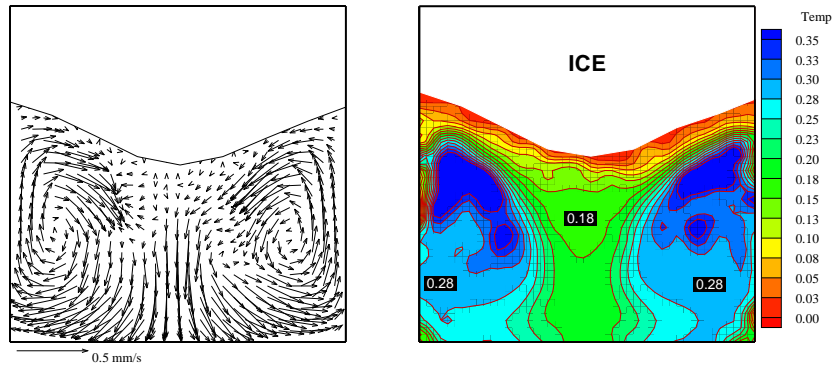


Fig. 5. Velocity (*left*) and non-dimensional temperature (*right*) field evaluated for water freezing in the lid cooled cavity after 5 hours, $T_h=20^\circ\text{C}$, $T_c=-10^\circ\text{C}$

the existence of a complex spiralling structure transporting fluid up along the side walls and down in a central cold jet along the cavity axis. A colour play of TLCs seeded flow images taken directly under the lid shows this flow structure in the temperature pattern. Both the particle tracks and temperature distribution measured underneath the lid indicate the existence of eight symmetric cells created by the flow (comp. Fig. 6). This is also manifested in the complex structure of the ice surface. In both the computed and observed ice surface, a star-like grooving reflects eight-fold symmetry of the flow [6]. It was found that heat flux through, as well as along the walls has to be incorporated in the numerical model to obtain observed flow pattern. It was only as a result of the use of both the experimental and numerical methods that the fine structures of the thermal flow were fully understood.

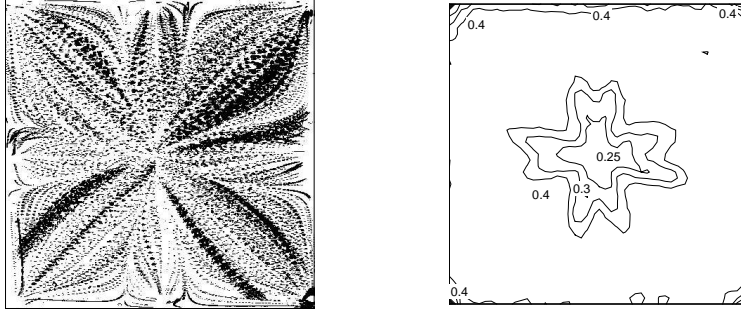


Fig. 6. Flow structure observed for the horizontal plane ($y=0.9$) underneath the cooled lid; particle tracks (*left*) and non-dimensional temperature isotherms evaluated from the colour of TLC tracers (*right*)

5 Conclusions

The present study has demonstrated the applicability of cholesteric liquid crystals to the quantitative measurements of full field instantaneous temperature distribution in freezing water. The simultaneous measurement of the velocity and temperature fields using TLC tracers, allows a detailed experimental description of the complex flow structures appearing in the convective flow associated with phase change, and their direct comparison with the numerical counterparts. Several discrepancies found between predicted and observed flow indicates the necessity of careful experimental verification of the numerical codes used for simulating phase change problems. It seems that the presented experimental technique offers a valuable tool for the code validation procedure.

References

1. Kowalewski T. A. (1998) Experimental validation of numerical codes in thermally driven flows. *Adv. in Comput. Heat Transfer CHT-97*, 1–15, Begel House Inc., New York.
2. Hiller W., Kowalewski T. A. (1987) Simultaneous measurement of the temperature and velocity fields in thermal convective flows. *Flow Visualization IV*, 617–622, Hemisphere.
3. Qunot G., Pakleza J., Kowalewski T. A. (1998) Particle Image Velocimetry with Optical Flow. *Exp. in Fluids* **25**, 177–189.
4. Kowalewski T. A., Rebow M. (1999) Freezing of water in the differentially heated cubic cavity. *Int. J. of Comp. Fluid Dyn.* **11**, no. 3-4, 193–210.
5. Kowalewski T. A., Cybulski A. (1996) Experimental and numerical investigations of natural convection in freezing water. *Int. Conf. on Heat Transfer with Change of Phase*, Kielce, *Mechanics* **61/2**, 7–16.
6. Kowalewski T. A., Cybulski A. (1997) Natural convection with phase change (in polish). *IPPT Reports* **8/97**, IPPT PAN, Warszawa.